ELSEVIER

Journal of Chromatography A, 797 (1998) 121–131

JOURNAL OF CHROMATOGRAPHY A

Effect of domain size on the performance of octadecylsilylated continuous porous silica columns in reversed-phase liquid chromatography

Hiroyoshi Minakuchi[a], Kazuki Nakanishi[a], Naohiro Soga[a], Norio Ishizuka[a], Nobuo Tanaka[b,*]

[a]*Kyoto University, Division of Material Chemistry, Faculty of Engineering, Yoshida, Sakyo-ku, Kyoto 606-01, Japan*
[b]*Kyoto Institute of Technology, Department of Polymer Science and Engineering, Matugasaki, Sakyo-ku, Kyoto 606, Japan*

Abstract

We prepared continuous porous silica columns having double pore structures with micrometer-size co-continuous through-pores and silica skeletons which have mesopores. The through-pore volumes and the ratio of through-pore diameters to silica skeleton diameters were kept constant, and the domain sizes were varied between 2.3 and 5.9 μm. We examined the effect of the domain size on the performance of silica rod columns in reversed-phase liquid chromatography after octadecylsilylation. The rod column having a smaller domain size showed lower plate height, though not so low as expected based on their skeleton size, and a smaller effect of linear velocity of mobile phase on the plate height for alkylbenzenes. The tendency was more pronounced for a larger molecule such as insulin. It was found that flow resistance parameters and separation impedance of the rod columns were smaller than those of conventional packed columns by a factor of 5 or more and showed little dependence on the domain size. The silica monoliths with double pore structure can provide a higher efficiency at a lower back pressure than conventional particle-packed columns.

Keywords: Silica; Pore size; Domain size; Stationary phases, LC

1. Introduction

Silica-based packing materials for reversed-phase HPLC have been extensively studied and widely used for analyzing and purifying various compounds. In conventional HPLC, the columns are packed with porous particles to provide large surface areas and high sample loading capacity. The interparticle mass transport is effected by rapid convection in these columns, while mass transport within particles takes place entirely based on molecular diffusion, which is very slow relative to convection, especially for macromolecules [1–3]. Since the difference in time required for a solute to travel intra- and inter-particle spaces becomes progressively greater as the linear velocity of the mobile phase becomes higher, it is necessary to make the particles smaller and to shorten the time required to diffuse within a particle. Large numbers of theoretical plates per unit time can be obtained by using small particles under high pressure [4–6]. However, the back pressure is inversely proportional to the particle size squared. It is possible to lower the back pressure and to increase diffusion coefficients by operating the column at very high temperatures [7,8], although this approach needs specially designed equipment. Consequently the use of small particles of less than 2 μm has been

*Corresponding author.

0021-9673/98/$19.00
PII S0021-9673(97)00947-3

limited, and capillary electrochromatography utilizing small particles is intensively studied.

A possible solution to the problem of a high back pressure associated with small particles is to make the diffusion path length shorter while maintaining the size of the convection path. Afeyan and co-workers reported the use of packing materials that contain very large pores with sizes up to 800 nm, which allow some of the mobile phase to flow through the particles, in addition to the pores with sizes similar to those of standard packing particles [9,10]. It has also been attempted to use continuous porous polymer beds as separation media [11–18]. These columns showed high-speed separation of polypeptides and proteins in reversed-phase and in ion-exchange chromatography. They showed that the efficiency of the separation was almost independent of the flow-rate and that the back pressure was modest even at high flow-rates. However, it is not easy to obtain high efficiency for small molecules with continuous beds made of organic materials [16–18].

Nakanishi and co-workers recently reported that silica gel monoliths could be prepared with a broad range of well-defined, controllable pores in the micrometer range, called 'through-pores', as well as with nanometer range mesopores [19–22]. The silica monoliths with double pore structures were prepared by a sol–gel method from alkoxysilanes in the presence of water-soluble organic polymers. In this system, spinodal decomposition occurs concurrently with gelation due to hydrolytic polymerization of alkoxysilanes, resulting in the formation of bicontinuous silica-rich and solvent-rich phases. After drying and thermal treatment of the wet gel, the silica-rich phase becomes mesoporous silica skeletons and the solvent-rich phase becomes through-pores. In this double-pore silica gel, the through-pore size and the silica skeleton size can be controlled independently by changing the composition of the starting mixtures.

We previously reported the effect of skeleton size on the performance of octadecylsilylated porous silica rods with constant through-pore sizes [23]. The silica rods with 1.0–1.7-μm skeletons and 1.5–1.7-μm through-pores provided high column efficiencies at a high mobile phase velocity and a smaller pressure drop as compared to columns packed with 5-μm particles. The silica rods with smaller skeletons showed little decrease in efficiency at a high mobile phase velocity. These features were provided by the small skeletons and the large through-pores with a ratio of through-pore size to silica skeleton size of about unity or even larger. Typically the ratio of the interstitial void size to the particle diameter is 0.25–0.4 for a particle-packed column [24]. In this study we kept the ratio of the through-pore size to the silica skeleton size nearly constant at ca. 1.3–1.4, and examined the effect of the domain size, that is the unit length of the spinodal decomposition structure, on the performance of the silica rod columns.

2. Experimental

2.1. Preparation of continuous porous silica columns

Tetramethoxysilane, TMOS (Tokyo Kasei, Tokyo, Japan), was used as a silica source. Poly(ethylene oxide), PEO (Aldrich, Milwaukee, WI, USA), having a molecular mass of 10 000 was used as a polymer component. Aqueous solution (0.01 *M*) of acetic acid (Nacalai Tesque, Kyoto, Japan) was used as a catalyst for hydrolysis.

Starting compositions are shown in Table 1. Only the amount of PEO was varied in order to produce silica monoliths with various domain sizes by following the procedure described previously [21,23]. PEO was dissolved in acetic acid, to which TMOS was added and stirred vigorously, and the mixture was homogenized. The solution was then poured into a polycarbonate mold (300×9 mm I.D.) and kept at 40°C for phase separation and gelation, then aged for a total of 15 h. In order to obtain appropriate nm-size mesopores, the silica monoliths were subsequently immersed in a 0.01 or 1.0 *M* aqueous ammonium hydroxide solution at 120°C for 9 h. After the treatment with a 0.1 *M* aqueous nitric acid solution, the silica monoliths were dried at 50°C for 3 days and finally heat-treated at 700 for 2 h.

2.2. Characterization of pore properties

A scanning electron microscope (SEM S-510,

Table 1
Composition of the preparation mixtures and the concentration of ammonium hydroxide, and the pore properties of the silica rods

Silica rod no.	Amount of PEO[a] (g)	NH_4OH[b] (mol/l)	Mesopore size[c] (nm)	Domain size[d] (μm)	Through-pore size[e] (μm)
SR-(A)-L	9.4	1.0	25.2	5.88	3.46
SR-(A)-S	9.4	0.01	15.7	5.70	3.39
SR-(B)-L	9.8	1.0	25.2	3.85	2.18
SR-(B)-S	9.8	0.01	15.8	3.81	2.23
SR-(C)-L	10.2	1.0	23.2	2.97	1.68
SR-(C)-S	10.2	0.01	13.1	2.89	1.73
SR-(D)-L	10.4	1.0	23.6	2.27	1.28
SR-(D)-S	10.4	0.01	15.5	2.32	1.26

[a]PEO added to 45 ml of TMOS and 100 ml of 0.01 *M* aqueous acetic acid.
[b]Concentration of NH_4OH used for controlling the mesopore size.
[c]Measured by nitrogen adsorption.
[d]Measured from SEM photographs as the sum of the size of an isolated through-pore and the size of a surroundng silica skeleton.
[e]Measured by mercury porosimetry. The skeleton size can be estimated by subtracting the through-pore size from the domain size.

Hitachi, Japan) was employed to observe the morphology of the resultant silica monoliths. Mercury porosimetry (Poresizer 9320, Micromeritics, USA) and nitrogen adsorption method (ASAP 2000, Micromeritics) were used to characterize the through-pores and the mesopores, respectively, of continuous porous silica columns.

2.3. Chromatography

Double-pore silica rods of 7.0 mm diameter, 83 mm in length were octadecylsilylated by on-column reaction, as previously reported [22,23], and used in a Z-module (Waters, Milford, MA, USA) under applied external pressure of ca. 100 kg cm^{-2}.

Chromatography was carried out using a conventional HPLC system consisting of an LC-10A pump (Shimadzu, Kyoto Japan), an injection valve fitted with a 20-μl sample loop (Model 7125, Rheodyne, Berkeley, CA, USA), an SPD-6A UV detector (Shimadzu), and a C-R5A data processor (Shimadzu). Conventional columns (150×4.6 mm I.D.) packed with 5-μm silica C_{18} particles were obtained from commercial sources; Capcellpak C_{18} UG (pore size, 12 mm, Shiseido, Tokyo, Japan, Capcellpak C_{18} SG (pore size, 30 nm) and Deltabond ODS (pore size, 30 nm, Keystone Scientific, Bellefonte, PA, USA). Mobile phase was prepared from LC-grade solvents. Insulin (bovine pancreas) was obtained from Sigma (St. Louis, MO, USA). Chromatographic measurements were carried out at 30°C. In order to examine the pore structures chromatographically, size-exclusion chromatography (SEC) was performed with the rod columns and a packed column in tetrahydrofuran with alkylbenzenes and polystyrene standards with molecular masses ranging from 760 to 20 000 000.

3. Results and discussion

3.1. Pore properties of continuous porous silica gels

SEM photographs of the continuous porous silica rods in Fig. 1 show that both the silica skeletons and the through-pores are co-continuous and the domain size decreases with the increase in PEO content in the feed. The macroporous structures were formed by the sol–gel transition accompanied by spinodal decomposition, by which the periodic domains were developed from the initially homogeneous solution, and frozen by gelation. The size of the periodic domains, a unit size combining silica phase and solvent phase, mainly depends on the onset of phase separation relative to the occurrence of sol–gel transition [19–21]. The timing for the phase separation is delayed by the increase in PEO content, resulting in the smaller domain size.

Fig. 2 shows the through-pore size distribution measured by mercury porosimetry. The sharp distributions of the pore sizes around 1.3, 1.7, 2.3 and 3.4 μm were formed when the amounts of PEO were

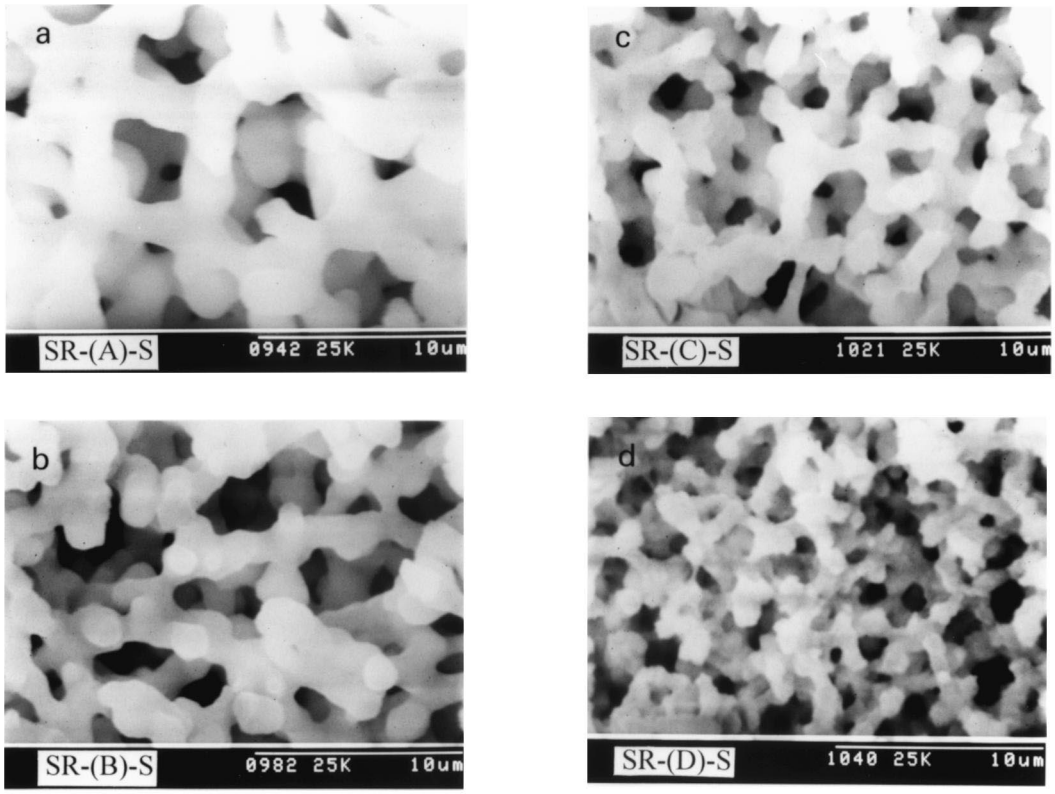

Fig. 1. SEM photographs of the gel morphologies. (a) SR-(A)-S, (b) SR-(B)-S, (c) SR-(C)-S, (d) SR-(D)-S.

10.4, 10.2, 9.8 and 9.4 g in the feed, respectively, as shown in Table 1, with a constant pore volume of ca. 3.2 cm^3 g^{-1}. Since these micrometer-range structures were formed by spinodal decomposition, the structures of skeletons and voids were expected to have self similarity [25,26]. Therefore, when the concentration ratio of TMOS to acetic acid was kept constant with a minor change in PEO content, the ratio of the silica skeleton size to the through pore size was constant and all the silica rods were also expected to have the same through-pore volume. The results indicate that all rods had similar through-pore volumes and ratios of silica skeleton size to through-pore size.

Fig. 3 shows the relation between domain size and through-pore size of the silica monoliths prepared in this study. Domain size, sum of the size of a through-pore and the size of the neighboring silica skeleton measured along two lines perpendicular to each other at 80 places for 40 through-pores, for each rod on SEM photographs, represents a unit structure in a rod-type column which possesses larger pores than silica skeletons. Average skeleton size can be calculated by subtracting the average through-pore size measured by mercury porosimetry from the domain size. Also plotted in Fig. 3 are the results of the previous study [23] and those with conventional columns packed with spherical particles. In conventional columns, the size of interstitial voids are reported to be 25–40% of the particle size [24]. As shown in Fig, 3, the silica monoliths have realized a column with large through-pores and small-sized skeletons.

Fig. 4 shows the size distributions of the mesopores measured by nitrogen adsorption method. The gels treated with a 0.01 or 1.0 *M* aqueous ammonium hydroxide solution possess pores distributed around 16 and 24 nm with surface areas of 340 and 140 m^2 g^{-1} and pore volumes of 0.96 and 0.90 cm^3 g^{-1}, respectively. These values were similar to those of

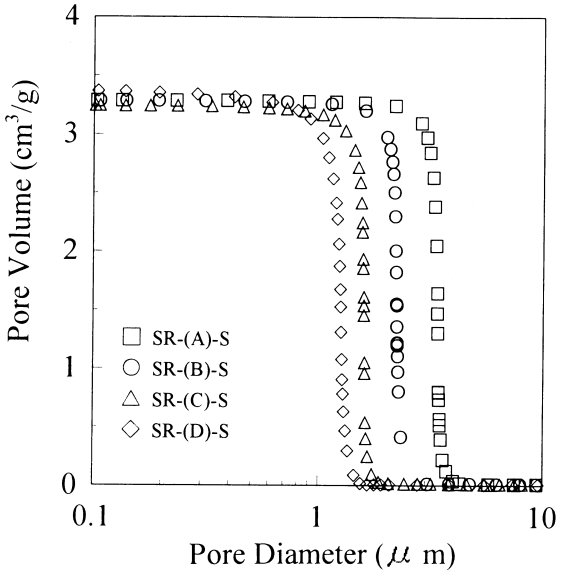

Fig. 2. Pore-size distribution curves of silica rods measured by mercury porosimetry. □, SR-(A)-S; ○, SR-(B)-S; △, SR-(C)-S; ◇, SR-(D)-S.

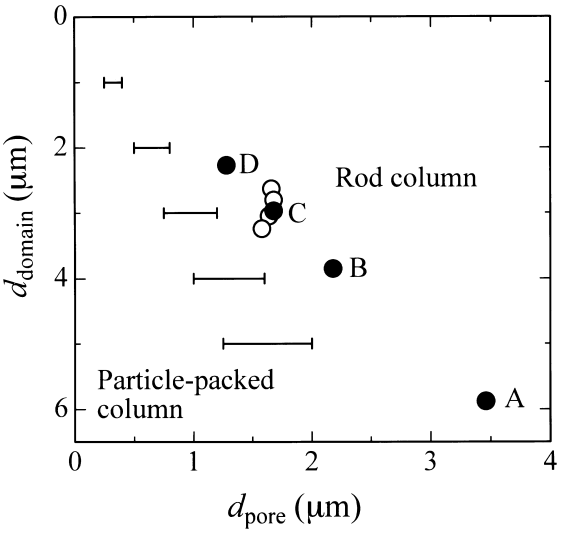

Fig. 3. Plots of the domain size against the through-pore size of the continuous silica columns having constant skeleton size/through-pore size ratio in this study (●), and those having constant through-pore size in a previous study [23] (○). Also plotted are the particle sizes (vertical axis) against the size of interstitial voids (25–40% of d_p as indicated by the bars) found with conventional particle-packed columns.

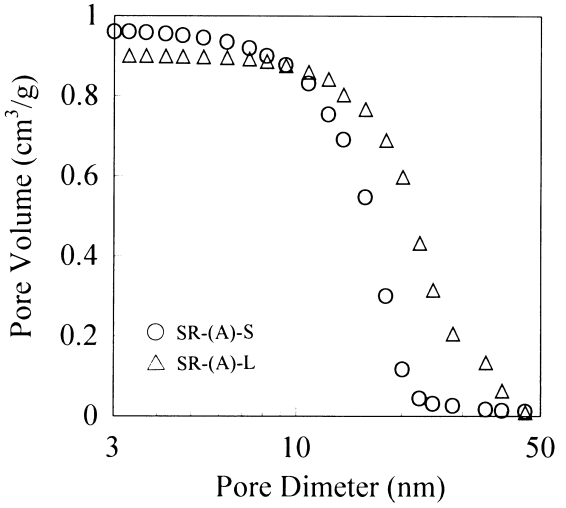

Fig. 4. Pore size distribution curves of mesopores in the silica skeletons measured by nitrogen adsorption. ○, SR-(A)-S; △, SR-(A)-L.

the silica-gel particles used for HPLC [24]. The results show the successful control of mesopore size up to 25 nm by changing pH and temperature in the solvent exchange process [23].

In Table 2, a noticeable difference was found between the rod columns and the packed column in the external porosity as measured by SEC. In the rod columns, the through-pore volume was nearly constant at ca. 62%. The ratio of the through-pore size to the silica skeleton size is about 1.2–1.5. In the case of the packed column, the interstitial void volume was ca. 40%, and the average size of the interstitial voids is much smaller than the particle size. A high external porosity and a large through-pore size of the rod column are important for the operation at a higher mobile phase velocity with a moderate back pressure.

SR-(C)-S and SR-(D)-S possess mesopores occupying 63 and 65% of apparent volume of silica, respectively, compared to 61% in the case of the silica particle. The volumes of mesopores of SR-(C)-S and SR-(D)-S were reduced by ca. 25 and 24%, respectively, by ODS modification, compared to 27% reduction in the silica particles. The results imply a similarity between the mesopore structure of the silica skeleton in the silica rod and that of the commercial silica particles. The silica skeleton in

Table 2
Pore volumes in rod columns and in a packed column obtained from SEC

	Pore volume (%) in a column					
	Rod column				Packed column[a]	
	SR-(C)-S		SR-(D)-S		Develosil	
	Silica	ODS	Silica	ODS	Silica	ODS
Through-pore volume[b]	62	63	61	62	39	39
Mesopore volume	24	18	25	19	37	27
Total pore volume	86	80	86	81	76	66
Silica skeleton volume[c]	38	—	39	—	61	—
Silica volume	14	—	14	—	24	—

[a]Develosil (Nomura Chemical, Seto, Japan; particle size, 5 μm; pore size, 11 nm).
[b]Interstitial void volume in the case of a particle-packed column.
[c]Apparent volume of silica skeleton with mesopores.

particles accounts for ca. 24% of column volume in the conventional packed column, while only 14% of the column volume is occupied by the skeleton in the silica monoliths. It becomes increasingly harder to prepare silica monoliths having a higher ratio of through-pore size to silica skeleton size, because such monoliths lose mechanical strength, as they become more porous.

3.2. Chromatographic performance of C_{18} continuous porous silica columns

Effect of a domain size on the chromatographic performance of C_{18} silica rods was examined with the elution of alkylbenzenes in 80% methanol, and with insulin in acetonitrile–water mixtures in the presence of trifluoroacetic acid (TFA). Eq. (1) relates the plate height to the mobile-phase velocity for a particle-packed column [1];

$$H = \frac{1}{\frac{1}{C_e d_p} + \left(\frac{1}{(C_m d_p^2 u)/D_m}\right)} + \frac{C_d D_m}{u} + \frac{C_{sm} d_p^2 u}{D_m} \quad (1)$$

where H is a plate height, d_p a particle diameter, u linear velocity of the mobile phase, D_m a diffusion coefficient of the solute, C_e, C_m, C_d, and C_{sm} coefficients representing the contribution of eddy diffusion, mobile-phase mass transfer, longitudinal diffusion, and mass transfer within a particle, respectively. At high mobile phase velocity the second term of Eq. (1) is negligible and the first term is nearly constant, which predicts a linear dependence of the plate height on the velocity. In this region the slope of the H vs. u plots is expected to be proportional to the square of the particle diameter for packed columns and proportional to the square of the skeleton diameter for rod columns.

The van Deemter plots obtained with amylbenzene as a solute in 80% methanol are shown in Fig. 5. The plots with TSKgel Super-ODS (particle diameter, 2 μm; pore size, 11 nm, Tosoh, Yamaguchi, Japan)

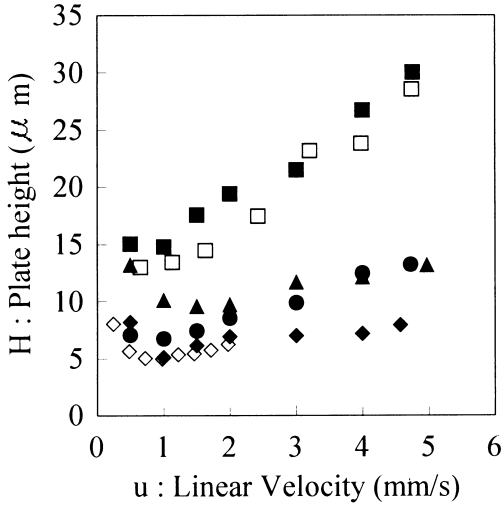

Fig. 5. Van Deemter plots for C_{18} silica rod columns and C_{18}-packed columns with amylbenzene as a solute. Mobile phase: 80% methanol. ■, SR-(A)-S-C_{18}; ●, SR-(B)-S-C_{18}; ▲, SR-(C)-S C_{18}; ♦, SR-(D)-S-C_{18}; □, Capcellpak C_{18} UG (12 nm); ◇, TSKgel Super ODS (from Ref. [5]).

obtained from Ref. [5] are also shown in Fig. 5. The performance of the SR-(A)-S-C_{18} was similar to that of 5-μm Capcellpak C_{18} UG particles, and SR-(B)-S-C_{18} showed an increase in efficiency as expected from the decrease in domain size. On the other hand, the performance of SR-(C)-S-C_{18} and SR-(D)-S-C_{18} was much lower than expected based on their pore and skeleton sizes, though SR-(D)-S-C_{18} showed comparable performance with 2-μm TSKgel Super-ODS particles. The slopes of the plots at high linear velocities decreased with reduced domain sizes reflecting the shorter diffusion path length.

Fig. 6 shows the Van Deemter plots obtained with insulin of molecular mass ca. 5800 as a solute in acetonitrile–water mixtures. The compositions of acetonitrile–water mixtures were adjusted to give similar k' values for insulin on each column, as the difference in retention time is too much at constant acetonitrile concentration. Since the diffusion in the mesopore is slower for a large molecule such as insulin, the influence of the third term in Eq. (1) to the column efficiency increases, thus the particle diameter or the silica skeleton size seriously affects the column efficiency, especially at high flow velocities. Fig. 6 indicates that all silica rods had smaller plate heights than the columns packed with 5-μm particles and the rods with smaller skeletons gave lower plate heights. It can also be seen in Fig. 6 that the plate heights increased linearly with the increase in the mobile phase velocity. This suggests that the contribution of the second term in Eq. (1) to the plate height can be ignored in this region of the plots for a large molecule.

Fig. 7 shows the relationship between the square of the diameter of the silica skeletons or the through-pores and the slopes of the plots (H vs. u) obtained from Fig. 6 at high-velocity regions. The linearity seen in the two sets of plots in Fig. 7 indicates that the ratio of the silica skeleton sizes to the through-pore sizes of all silica rods were nearly constant.

3.3. Column pressure drop

Fig. 8 shows the column back pressure against linear velocity of the mobile phase. The back pressure of SR-(A)-S-C_{18}, which had a comparable plate height to the 5-μm particle-packed column, as shown in Fig. 5, was lower than that expected for a column packed with 10-μm particles. The back pressure of

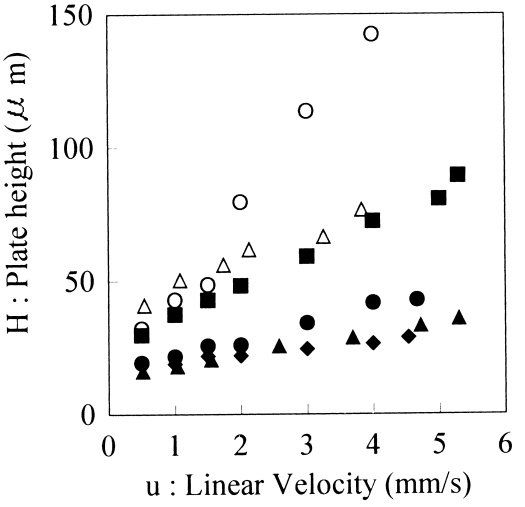

Fig. 6. Van Deemter plots for C_{18} silica rod columns and C_{18}-packed column with insulin as a solute. Mobile phase: acetonitrile–water (30:70) for rod columns, (32:68) for Capcellpak C_{18} SG, and (33.5:66.5) for Deltabond ODS (30 nm) in the presence of 0.1% trifluoroacetic acid. ■, SR-(A)-L-C_{18}; ●, SR-(B)-L-C_{18}; ▲, SR-(C)-L-C_{18}; ♦, SR-(D)-L-C_{18}; ○, Capcellpak C_{18} SG (30 nm); △, Deltabond ODS (30 nm).

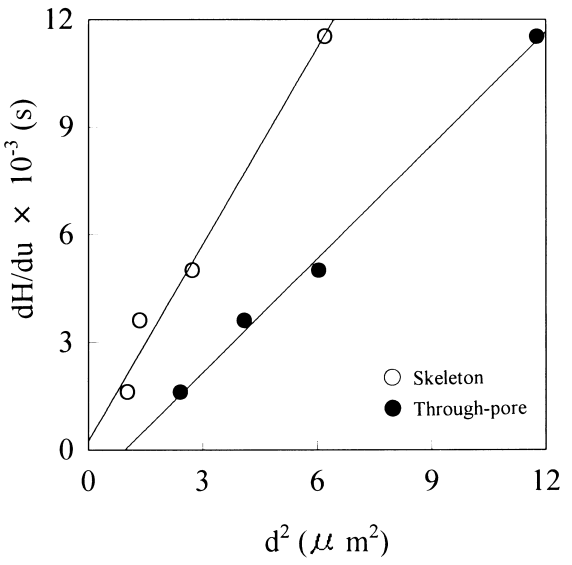

Fig. 7. Plots of slopes of the Van Deemter plots in Fig. 6 against skeleton size squared and through-pore size squared for the wide-pore rod columns with insulin as a solute. ○, skeleton size; ●, through pore size.

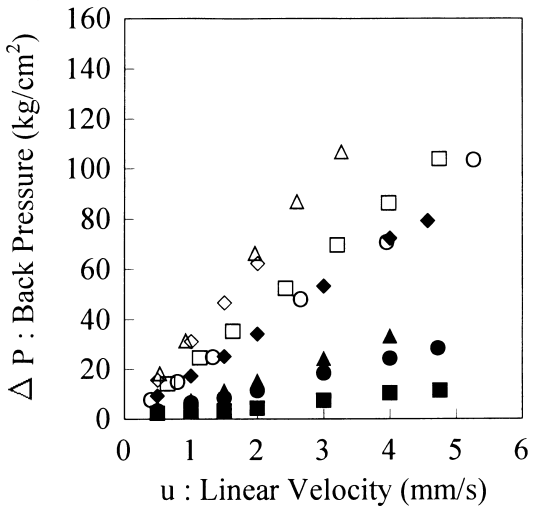

Fig. 8. Plots of column back pressure against linear velocity of mobile phase. Mobile phase: 80% methanol. The pressures were normalized to the column length of 83 mm. ■, SR-(A)-S-C_{18}; ●, SR-(B)-S-C_{18}; ▲, SR-(C)-S C_{18}; ♦, SR-(D)-S-C_{18}; □, Capcellpak C_{18} UG (12 nm); ○, Capcellpak C_{18} SG (30 nm); △, Deltabond ODS (30 nm); ◇, TSKgel Super ODS.

SR-(D)-S-C_{18}, which showed a small theoretical plate height similar to the column packed with 2-μm particles, was almost the same as that of a column packed with 5-μm particles. TSKgel Sper-ODS showed a low pressure drop comparable with 5-μm Deltabond ODS.

The permeability of the rod columns can be compared with the packed columns by using the dimensionless flow resistance parameter, ϕ. The permeability, K, for the bed made of uniformly sized spheres of diameter, d_p, is given by the Kozeny-Carman equation as follows [27];

$$K = \frac{\epsilon^3}{180(1-\epsilon)^2} \cdot d_p^2 \quad (2)$$

and the permeability is related to column pressure drop by Eq. (3), [28];

$$K = \frac{u\eta L}{\Delta P} \quad (3)$$

where ϵ is interstitial porosity, η viscosity of the mobile phase, L column length, and ΔP back pressure. For the bed made of cylinders of diameter d_c, d_p in Eq. (2) is replaced by $(3/2)d_c$ [27]. ϕ is related to K by Eq. (4) [28].

$$\phi = \frac{d_p^2}{K} \quad (4)$$

K and ϕ calculated from Eq. (2), Eq. (3), and Eq. (4) are shown in Table 3. The ϕ values were nearly constant with the rod columns. The results indicate that all rods had a similarity in structure in terms of the ratio of the through-pore size to the silica skeleton size, with constant through-pore volume. Flow-resistant parameters, ϕ values, of the rod columns were smaller than those of the packed column by a factor of 6–8. It is obvious that the rod columns which have co-continuous silica skeletons and through-pore structures can realize the performance of small particles at much lower back pressure than the particle-packed column.

It was proposed that the total column performance could be evaluated by the separation impedance, E value, [28] given by Eq. (5);

$$E = \frac{t_R \Delta P}{N^2 \eta (1+k')} \quad (5)$$

where t_R is elution time, N the number of theoretical plates, and k' the retention factor. Fig. 9 shows the separation impedance (E) calculated with amylbenzene as a solute for Capcellpak C_{18} UG and the rod columns with small mesopores against linear velocity

Table 3
Permeability and flow resistance parameter of rod columns and a packed column

	Permeability ($\times 10^{-14}$ m^2)		Flow resistance parameter	
	K^a	K^b	ϕ^c	ϕ^d
SR-(A)-S-C_{18}	26.4	40	131	86
SR-(B)-S-C_{18}	11.1	17	134	87
SR-(C)-S-C_{18}	6.6	13	127	64
SR-(D)-S-C_{18}	4.7	5.6	110	92
Capcellpak C_{18} UG	2.5	4.5	1010	520

[a]Calculated by Eq. (2). The through-pore volumes are measured by SEC. In the case of silica rods, the through-pores are considered to be cylinders.
[b]Calculated by Eq. (3).
[c]Calculated by Eq. (2) and Eq. (4).
[d]Calculated by Eq. (3) and Eq. (4), and the domain size was used as d_p for rod columns.

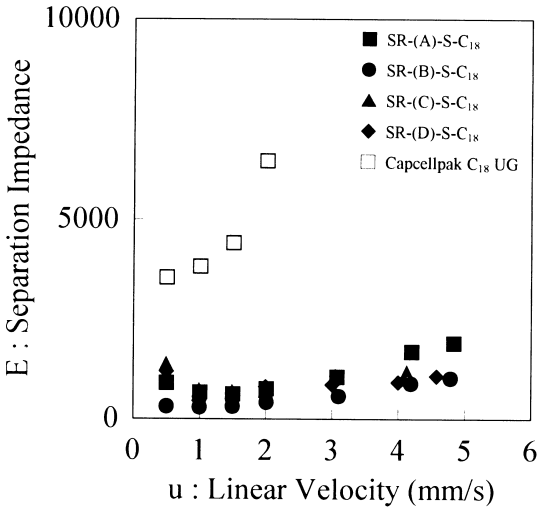

Fig. 9. Plots of separation impedance against linear velocity of mobile phase calculated for amylbenzene as a solute. (a) ■, SR-(A)-S-C_{18}; ●, SR-(B)-S-C_{18}; △, SR-(C)-S C_{18}; ♦, SR-(D)-S-C_{18}; □, Capcellpak C_{18} UG (12 nm).

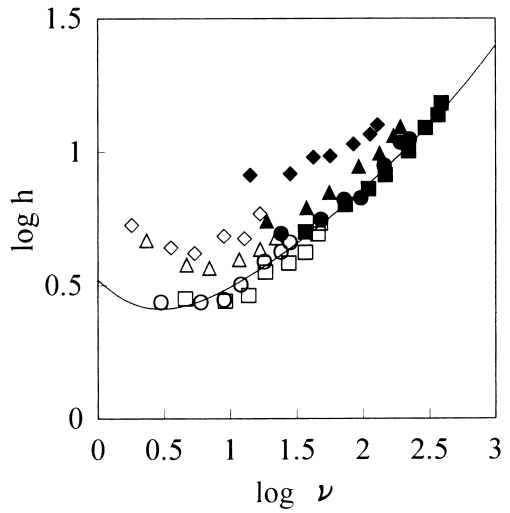

Fig. 10. Logarithmic plots of reduced plate height against reduced velocity for the wide-pore rod columns with insulin (solid symbols) and amylbenzene (open symbols) as solutes. □,■, SR-(A)-L-C_{18}; ○,●, SR-(B)-L-C_{18}; △,▲, SR-(C)-L-C_{18}; ◇,♦, SR-(D)-L-C_{18}. The solid curve shows the values calculated for $h = 1.3\upsilon^{1/3} + 2.0/\upsilon + 0.012\ \upsilon$.

of the mobile phase. The minimum E for Capcellpak C_{18} UG was approximately 3500, while minimum values of 300–700 were obtained for the rod columns. The difference in E values between the packed column and the rod columns becomes larger at higher linear velocity. Greater differences were seen between the rod columns and the particle-packed columns for insulin.

3.4. Estimation of optimum domain size

The dependence of the plate height on the mobile phase velocity is presented by Eq. (6) using the dimensionless reduced parameters [3,28];

$$h = A\upsilon^{1/3} + B/\upsilon + C\upsilon \quad (6)$$

where h is the reduced plate height, $h = H/d_p$, and υ is the reduced velocity, $\upsilon = ud_p/D_m$. The logarithmic plots of h against υ, obtained from the results with silica rods SR-(A)-L-C_{18}–SR-(D)-L-C_{18}, are shown in Fig. 10. The domain size, d_{domain}, was used as a size of the unit structure instead of d_p to calculate h and υ for the rod columns [23]. Since all rod columns have similarity in the internal structure, they are expected to have common A, B and C values, as is the case with particles prepared by one preparation method [28].

Fig. 10 indicates that, with a decrease in the domain size, higher h values were observed. The silica rods with smaller domain sizes did not provide the higher efficiency expected. The plots indicated that the coefficient A increased and C decreased with the decrease in the domain size, suggesting that SR-(C)-L-C_{18} and SR-(D)-L-C_{18}, with their smaller domains, have less regularity than SR-(A)-L-C_{18} and SR-(B)-L-C_{18} which provided the common h–υ relation shown by the curve in Fig. 10. As seen in Fig. 1, the silica skeletons of smaller size, especially SR-(D)-S, possess rough surfaces suggesting an unstable state of phase separation during gel formation. The results suggest that well-made rod columns of small domains would provide better performance, because the presence of large through-pores does not seem to be the major factor for low efficiency, as shown by the results with SR-(A)-L-C_{18} and SR-(B)-L-C_{18}.

The values $A = 1.7$ and $C = 0.05$ were obtained for Capcellpak C_{18} SG, indicating its excellent performance. The plots for the well-made rod columns, SR-(A)-L-C_{18} and SR-(B)-L-C_{18}, in Fig. 10 gave

$A=1.3$ and $C=0.012$ for Eq. (6), assuming $B=2.0$ [29], as shown by the solid curve in Fig. 10. (The A and C values are probably underestimated to be compared with those of a particle-packed column due to the use of the domain size as d_p. Actually, these values with silica rods may not be directly compared with those with particle-packed columns due to the difference in geometry between the two types of columns [1]. This subject needs further study.) By using these values and the flow resistance parameter, $\phi=90$, one can estimate the effect of the domain size on the performance of rod columns under various conditions. In this estimation, we assumed the viscosity of the mobile phase to be 10^{-3} N m s^{-1}, corresponding to water, and the diffusion coefficient of the solute to be 10^{-9} m^2 s^{-1}, which were also employed by Knox in the optimization of the performance of a particle-packed column [29].

Table 4 gives the theoretical plate numbers, N, calculated for various domain sizes when the retention time of an unretained solute, t_0, was maintained at 100, 30, or 10 s. The ν value to give minimum h is calculated to be 3.0 for the rod columns and h_{min} is then 2.6, as realized by SR-(A)-L-C_{18} and SR-(B)-L-C_{18}. The present results suggest that the optimum performance can be achieved with a silica rod column of $d_{domain}=4.0$ μm at $t_0=100$ s. The preparation of a silica rod column corresponding to optimum domain size for operation at a higher pressure or a smaller t_0 value, however, needs improvement in the preparation conditions in order to achieve higher regularity of the structure to reduce the A term contribution. At present the silica rod columns having a domain size of less than 3 μm are not sufficient to show the optimum performance expected.

The possibilities with the silica rod columns shown in Table 4, however, are still notable in that (i) it is feasible to operate a long column with current instrumentation, for example, a silica rod column ($d_{domain}=3.5$ μm) of 1 m long can generate ca. 10^5 theoretical plates with $t_0=7$ min at $\Delta P=170$ kg cm^{-2}, (ii) it will be possible to achieve a separation with 10^4 theoretical plates and k' of up to 3–4 in 1 min at a ΔP of 50 kg cm^{-2}, if we can produce a silica rod column of 2 μm domain size, with the same quality that was achieved with the silica rod columns of larger domain sizes, SR-(A)-L-C_{18} or SR-(B)-L-C_{18}. The present preparation conditions seem to be optimum for the preparation of silica rod columns with ca. 60% external porosity and with relatively large domain sizes.

4. Conclusion

In the preparation of continuous silica columns with double-pore structure, we were able to keep the

Table 4
Number of theoretical plates calculated for the rod columns with $l=20\,000$, $\phi=90$, and $h=1.3\nu^{1/3}+2.0/\nu+0.012\nu$, for $\eta=10^{-3}$ N m s^{-1} and $D_m=10^{-9}$ m^2 s^{-1}

Domain size (μm)	1.0	1.5	2.0	2.5	3.0	3.5	4.0	4.5	5.0
($t_0=100$ s, $\Delta P=3.6$ kg/cm^2)									
ν	0.20	0.45	0.80	1.25	1.80	2.45	3.20	4.05	5.00
h	10.8	5.45	3.72	3.02	2.71	2.60	2.58	2.61	2.68
N	1860	3670	5380	6630	7370	7700	7750	7650	7450
L (mm)	20	30	40	50	60	70	80	90	100
($t_0=30$ s, $\Delta P=12$ kg/cm^2)									
ν	0.67	1.50	2.67	4.17	6.00	8.17	10..7	13.5	16.7
h	4.14	2.84	2.58	2.62	2.77	2.96	3.18	3.41	3.64
N	4830	7040	7740	7630	7230	6750	6290	5870	5490
L (mm)	20	30	40	50	60	70	80	90	100
($t_0=10$ s, $\Delta P=36$ kg/cm^2)									
ν	2.00	4.50	8.00	12.5	18.0	24.5	32.0	40.5	50.0
h	2.66	2.64	2.95	3.33	3.73	4.15	4.57	5.00	5.43
N	7510	7560	6790	6010	5360	4820	4370	4000	3680
L (mm)	20	30	40	50	60	70	80	90	100

ratio of through-pore size to silica skeleton size nearly constant at 1.2–1.4, and to control the domain sizes. The H_{min} value and the slope of the H–u plots decrease and the column back pressure increases with the decrease in domain size. We were able to prepare silica rod columns having domain sizes of 3.8 and 5.8 μm, which showed performances similar to those of 3- and 5-μm particles, respectively, with pressure drops lower than those with particle-packed columns by a factor of 6–8, although silica rod columns with domain sizes smaller than 3 μm showed somewhat lower performance than expected. The continuous silica columns will provide higher column efficiencies at much lower ΔP than particle-packed columns of comparable silica size, especially for high-molecular-mass solutes.

Acknowledgements

This work was supported in part by grant-in-aid for scientific research and Monbusho International Joint Research Program funded by the Ministry of Education, Science, Sports, and Culture.

References

[1] J.C. Giddings, Dynamics of Chromatography, Part 1, Principles and Theory, Marcel Dekker, New York, 1965.
[2] C. Horvath, H.-J. Lin, J. Chromatogr. 149 (1978) 43–70.
[3] G. Guiochon, in: C. Horvath (Ed.), High Performance Liquid Chromatography—Advances and Perspectives, vol. 2, Academic Press, New York, 1980.
[4] K.K. Unger, G. Jilge, J.N. Kinkel, M.T.W. Hearn, J. Chromatogr. 359 (1986) 61–72.
[5] H. Moriyama, M. Anegayama, K. Komiya, Y. Kato, J. Chromatogr. A 691 (1995) 81–89.
[6] J.E. MacNair, K.C. Lewis, J.W. Jorgenson, Anal. Chem. 69 (1997) 983–989.
[7] F.D. Antia, C. Horvath, J. Chromatogr. 435 (1988) 1–15.
[8] C. Chen, C. Horvath, Anal. Methods Inst. 1 (1993) 213–222.
[9] N.B. Afeyan, N.F. Gordon, I. Mazsaroff, L. Varady, Y.B. Yang, F.E. Regnier, J. Chromatogr. 519 (1990) 1–29.
[10] N.B. Afeyan, S.P. Fulton, F.E. Regnier, J. Chromatogr. 544 (1991) 267–279.
[11] J.L. Liao, S. Hjerten, J. Chromatogr. 457 (1988) 165–174.
[12] S. Hjerten, J.L. Liao, R. Zhang, J. Chromatogr. 473 (1989) 273–275.
[13] F. Svec, J.M. Frechet, Anal. Chem. 64 (1992) 820–822.
[14] Q.C. Ching, F. Svec, J.M.J. Frechet, Anal. Chem. 65 (1993) 2243–2248.
[15] Y.-M. Li, J.-L. Liao, K. Nakazato, J. Mohammad, L. Terenius, S. Hjerten, Anal. Biochem. 223 (1994) 153–158.
[16] C. Ericson, J.-L. Liao, K. Nakazato, S. Hjerten, J. Chromatogr. A 767 (1997) 33–41.
[17] C. Fujimoto, J. Kino, H. Sawada, J. Chromatogr. A 716 (1995) 107–113.
[18] Q.C. Ching, F. Svec, J.M.J. Frechet, J. Chromatogr. A 669 (1994) 230–235.
[19] K. Nakanishi, N. Soga, J. Am. Ceram. Soc. 74 (1991) 2518–2530.
[20] K. Nakanishi, Y. Sagawa, N. Soga, J. Non-Cryst. Solids 134 (1991) 39–46.
[21] K. Nakanishi, N. Soga, J. Non-Cryst. Solids 139 (1992) 1–24.
[22] H. Minakuchi, K. Nakanishi, N. Soga, N. Ishizuka, N. Tanaka, Anal. Chem. 68 (1996) 3498–3501.
[23] H. Minakuchi, K. Nakanishi, N. Soga, N. Ishizuka, N. Tanaka, J. Chromatogr. A 762 (1997) 135–146.
[24] K.K. Unger, Porous Silica, Elsevier, Amsterdam, 1979.
[25] T. Hashimoto, M. Itakura, H. Hasegawa, J. Chem. Phys. 85 (1986) 6118–6128.
[26] T. Hashimoto, M. Itakura, N. Shimidzu, J. Chem. Phys. 85 (1986) 6773–6786.
[27] M. Kaviany, Principles of Heat Transfer in Porous Media, Springer-Verlag, 1991.
[28] P.A. Bristow, J.H. Knox, Chromatographia 10 (1977) 279–289.
[29] J.H. Knox, J. Chromatogr. Sci. 15 (1977) 352–364.